Article

Corrosion Behavior of Stainless Steel in Seawater in the Presence of Sulfide

Senka Gudić [1,*], Ladislav Vrsalović [1], Ante Matošin [2], Jure Krolo [3], Emeka Emanuel Oguzie [4] and Aleš Nagode [5]

[1] Faculty of Chemistry and Technology, University of Split, Ruđera Boškovića 35, 21000 Split, Croatia
[2] INA-Industrija Nafte, d.d., Rafinerija Nafte Rijeka, 53 Urinj, 51221 Kostrena, Croatia
[3] Faculty of Electrical Engineering, Mechanical Engineering and Naval Architecture, University of Split, Ruđera Boškovića 32, 21000 Split, Croatia
[4] Africa Centre of Excellence in Future Energies and Electrochemical Systems (ACE-FUELS), Federal University of Technology Owerri, Owerri 460113, Nigeria
[5] Faculty of Natural Sciences and Engineering, University of Ljubljana, Aškerčeva 12, 1000 Ljubljana, Slovenia
* Correspondence: sgudic@ktf-split.hr; Tel.: +385-21-329-433

Abstract: The effect of temperature (from 288 to 308 K) and concentration of sulfide ions (up to 40 ppm) on the corrosion behavior of AISI 304L and AISI 316L stainless steels in seawater was studied with measurements of open-circuit potential, linear and potentiodynamic polarization, and electrochemical impedance spectroscopy. An increase in temperature and pollutant concentration negatively affects the corrosion stability of stainless steels at the open circuit (the resistance, compactness, and thickness of the surface layer decrease and the corrosion current increases), in the passive region (the passivation current increases, the depassivation potential decreases, and the passive potential region narrows), and in the transpassive potential region (the rate of metal dissolution increases). The occurrence of pitting corrosion on the surface of the samples was confirmed with optical microscopy and a non-contact 3D profilometer. A few large pits (depth 80–100 μm and width 100 μm) were formed on the surface of AISI 304L steel, while several smaller pits (depth 40–50 μm and width 50 μm) were formed on the surface of AISI 316L steel. With increasing temperature and sulfide ion concentration, the width, depth, and density of the pits increased on both steel samples. In the studied temperature and concentration range of sulfide ions, the AISI 316L steels exhibited higher corrosion resistance. Overall, the influence of sulfide ions on steel corrosion was more pronounced than the influence of temperature.

Keywords: stainless steel; seawater; sulfide; pitting corrosion; passive film; surface analysis

1. Introduction

Marine environments can be very challenging for metallic structural materials due to factors such as high salinity, water velocity, temperature, and biological activities [1–5]. The corrosion of alloys in seawater has serious effects on the reliability and service life of marine equipment, causing severe damage to structures, materials, equipment, port facilities, and ships, which is a major concern for scientists and engineers [6–8]. In addition to the adverse effects of chlorides and other halide ions naturally present in seawater, pollutants can also have a significant impact on the corrosion of metals.

Corrosion and pollution are interrelated processes, as many pollutants produced by burning fossil fuels accelerate corrosion, and corrosion products such as rust, oxides, and salts pollute water. Both processes negatively affect the quality of the environment and the durability of marine structures and building materials [7,9]. Pollution also leads to climate change, which can alter environmental conditions and increase the risk of corrosion failures, altered precipitation patterns, and the corrosiveness of coastal regions, with added stresses on marine systems [9,10]. Anthropogenic activities increase the generation of CO_2, H_2S,

and NH_3. Such contaminants may originate from natural geochemical processes, biological and bacteriological processes in seawater, and anthropogenic sources such as industrial waste discharge, oil and gas production, or scattered anoxic sediments [11–14]. Among these compounds, hydrogen sulfide (H_2S) is a highly toxic compound that accelerates the deterioration of steel structures in a process known as sour water corrosion.

While hydrogen sulfide is always present in anaerobic seawater, studies have shown that sulfides are also widespread in aerobic surface waters, usually at concentrations 4–6 orders of magnitude lower than in anoxic regions. In both anaerobic and aerobic water, hydrogen sulfide occurs as a dissolved gas [$H_2S(g)$], as its dissociated ions, bisulfite (HS^{2-}) and sulfide (S^{2-}), and as dissolved metal-sulfide complexes [12,13].

Metals and alloys used in oil and gas extraction and purification processes also suffer from severe corrosion due to the presence of sulfur-containing ions such as $S_2O_3^{2-}$, SO_3^{2-}, $S_2O_4^{2-}$, and HS^- together with H_2S [1,2]. H_2S is the most critical pollutant in seawater and can reach levels of 50 ppm or more in heavily polluted coastal or harbor waters [11]. Dissolved-free sulfides have been found to be very aggressive species towards many different metals and alloys, including various types of steels, copper and copper alloys, titanium and its alloys, etc. [11,15,16].

Syrett investigated the corrosion of Cu-Ni alloys in sulfide-contaminated seawater and found that the presence of dissolved sulfide in seawater leads to the formation of a porous copper sulfide corrosion product, which interferes with the normal growth of the protective oxide film and enables the initial high corrosion rate in aerated seawater [17]. Traverso et al. [18] studied the corrosion of CuNiFeMn alloys in sulfide-polluted and unpolluted natural seawater and found an accelerated corrosion attack at a sulfide concentration of 4 ppm. The presence of sulfur oxyanions deep in the corrosion layer leads to structural defects and the formation of poorly compact and porous corrosion product layers with low corrosion protection. Szprovwski [19] studied the corrosion of different types of steel in NaCl solution saturated with H_2S and observed that saturation of the chloride solution with H_2S gas further reduced the corrosion resistance of the steels since the presence of H_2S impeded passivation and lowered the breakdown potentials of all the steels studied. Moreover, Dexter [20] observed that the pitting corrosion of low-carbon steels in the polluted seawater of San Diego Harbor in California, SAD, was several times higher than the corrosion that normally occurs in clean seawater [20].

Although most of the published research results indicate a negative influence of sulfides on the corrosion of metals and alloys, there are also those showing the opposite influence, namely the positive effects of sulfides inhibiting corrosion under certain conditions by the formation of protective iron sulfide layers [21]. For instance, Zhao et al. found that sulfide film on the steel surface prevents pitting and the corrosion resistance increases with immersion time [22].

Stainless steels are widely used in marine structures, so the study of their behavior in seawater is of great interest. Austenitic stainless steel grades 304 and 316 have excellent ductility, good strength, nonmagnetic properties, good weldability, and very good corrosion resistance, so these materials find widespread practical applications [23–27]. Grade 304 stainless steel is commonly used as a material for marine fittings, while grade 316 stainless steel (UNS S31600/S31603—commonly referred to as marine stainless steel) is used in about 90% of marine applications. The high corrosion resistance of austenitic stainless steels is a consequence of the natural formation of a protective passive oxide layer on their surface with a high Cr content and a thickness of 1–10 nm [28–30]. Although the resistance of passive films to general corrosion is relatively high, they are susceptible to localized attack. Pitting corrosion is the most common form of electrochemical damage to stainless steel, caused by the local breakdown of the surface passive layer.

The susceptibility of metals and alloys to pitting corrosion depends on factors such as temperature and environmental composition. As with chemical reactions, the rate of pitting corrosion increases with increases in electrolyte temperature. Indeed, a strong dependence of pitting potential on temperature has been found in previous studies on stainless steel,

with higher pitting potentials observed at lower temperatures and lower pitting potentials at higher temperatures [31,32].

The presence of impurities such as sulfides and sulfur oxides in seawater has a negative effect on the passivation kinetics of stainless steel [33]. It has been suggested that sulfide and chloride may act synergistically in the film, with the integration of sulfide into the passive film facilitating further infiltration by chloride and promoting the formation of pits at surface inhomogeneities [34]. Mat and Newman [35] and later Marcus [36] proposed a mechanism by which sulfur species adsorbed on the pit surface maintain activity and retard repassivation, leading to the propagation of pits in stainless steels. Ding et al. [37] found that the passive film in Cl^- solution without sulfide has a variation of p/n semiconductor type, which can provide good protection for the film. However, the passive film in H_2S–Cl^- solutions exhibits only an n-type semiconductor behavior, which tends to attract anions to the film and impair its protective effect. The n-type semiconductor in H_2S–Cl^- solutions is caused by the sulfidation of oxides on the film.

Although the mechanism of H_2S-induced sour water corrosion of various alloys has been researched, some contradictory results and the high damage caused by corrosion in the presence of H_2S provide the impetus for further research on this topic.

In this work, we combined the results of electrochemical measurements with the results of surface characterization, which included optical and SEM/EDS microscopy and 3D profilometry, to compare the corrosion behavior of 304L and 316L stainless steels in seawater at different temperatures and different concentrations of Na_2S (10 and 40 ppm), to determine the form of corrosion attack, the depth of corrosion penetration into the material, and the elemental composition of corrosion products on the surface.

2. Materials and Methods

Stainless steel rods (AISI 304L and AISI 316L) with a diameter of 6 mm and a length of 150 mm were purchased from commercial sources (Ronsco, China) with the chemical composition listed in Table 1.

Table 1. Chemical composition of investigated stainless steels (in wt.%).

Sample	Cr	Ni	Mn	Mo	Si	Cu	C	Fe
AISI 304L	16.76	8.66	2.23	0.11	0.52	0.38	0.03	71.58
AISI 316L	16.47	10.54	1.16	2.53	0.47	0.27	0.002	68.55

The preparation of the electrodes for the electrochemical measurements from the steel rods has been described previously [26]. Before each measurement, the working surface of the electrode was ground with abrasive paper to a grit size of 2500 using a Metkon Forcipol 1V grinding and polishing machine and then polished with a diamond polishing suspension Metkon Diapat M (particle size 1 μm). The final processing step before immersion in the electrolyte was a 5-min ultrasonic cleaning in ethanol and deionized water.

The seawater for this study was collected at Žnjan beach in the city of Split, Croatia (coordinates: 43.5018° N, 16.4763° E). The physical parameters of the seawater used as a test environment are listed in Table 2, and the chemical composition of the seawater is listed in Table 3.

Table 2. The physical parameters of the seawater used for the experiments.

Medium	pH	Conductivity $(mS\ cm^{-1})$	Salinity (ppt)	Dissolved Oxygen $(mg\ L^{-1})$
Seawater	8.10	57.7	38.5	5.4

Table 3. The approximate chemical composition of seawater (main ions).

Ions	Cl^-	Na^+	SO_4^-	Mg^{2+}	Ca^{2+}	K^+	Br^-	Sr^{2+}	F^-
mg L^{-1}	21846	12168	2958	1409	453	439	74	9	1

To prepare seawater solutions with a sulfide content of 10 and 40 ppm, the mass of Na_2S salt p.a. purity was calculated, weighed on an analytical balance, and, finally, dissolved in a given volume of seawater in a volumetric flask.

A three-electrode double-walled glass cell containing the working electrode, Ag/AgCl as the reference electrode, and a Pt-sheet counter-electrode was used for the electrochemical measurement. The Huber Kiss K6 cooling bath thermostat was connected to a cell to maintain the desired operating temperatures (288, 298, and 308 K).

An EG&G Princeton Applied Research Model 273A potentiostat-galvanostat was used for the electrochemical measurements along with a PAR M 5210 lock-in amplifier (Princeton, NJ, USA) for the electrochemical impedance measurements (EIS).

The open circuit potential (E_{OC}) was recorded every 20 s after the working electrode was immersed in the electrolyte for 60 min. EIS measurements were performed at the E_{OC}, with the voltage perturbation amplitude of 10 mV in the frequency range from 50 kHz to 30 mHz with 5 points per decade. Linear polarization resistance (LPR) measurements were recorded in a potential range of ±20 mV versus E_{OC} with a scan rate of 0.2 mV s^{-1}. Potentiodynamic polarization measurements (PD) were carried out with a scan rate of 1 mV s^{-1} starting from -250 mV versus E_{OC} up to 800 mV. All electrochemical measurements were performed in triplicate to ensure the reproducibility of results.

The optical microscope MXFMS-BD (Ningbo Sunny Instruments Co., Ningbo, China) with $100\times$ magnification was used to examine the corroded steel surfaces after the potentiodynamic polarization measurements, and the depth of pitting corrosion was examined with a Profilm3D 3D optical profilometer (KLA Corporation, Milpitas, CA, USA). Prior to these surface examinations, the electrode surfaces were immersed in deionized water, cleaned in an ultrasonic bath for 5 min, and then dried in a laboratory dryer at a temperature of 323 K.

The morphology of the corrosion products and the elemental composition in some characteristic areas of the sample surfaces were determined using a field emission scanning electron microscope (FEG SEM) Thermo Scientific Quattro S (FEG SEM, Hillsboro, OR, USA) connected to an EDS SDD Ultim®Max detector, Oxford Instruments, for semi-quantitative analysis. For SEM/EDS analysis, the electrode surfaces were dried without ultrasonic cleaning.

3. Results and Discussion

3.1. Open Circuit Potential Measurement

Figure 1 shows the time dependence of the open circuit potential (E_{OC}) for AISI 316L in seawater at different experimental conditions (different temperatures and different S^{2-} concentrations).

The E_{OC} is a result of the electrochemical reactions that take place at the stainless steel/seawater interface. As can be seen, the E_{OC} value depends strongly on the experimental conditions: the composition of the stainless steel, the properties of the seawater (temperature and presence of S^{2-} ions), and the immersion time. Immediately after immersion in seawater at 288 K, AISI 316L steel reaches a potential of ≈-45 mV, which becomes more positive with time (due to the formation and thickening of the protective passive film on the electrode surface) [38,39], and after about 10 min a more or less stable value of ≈-15 mV is established (Figure 1a). As the temperature of the seawater increases, the final E_{OC} value becomes more negative.
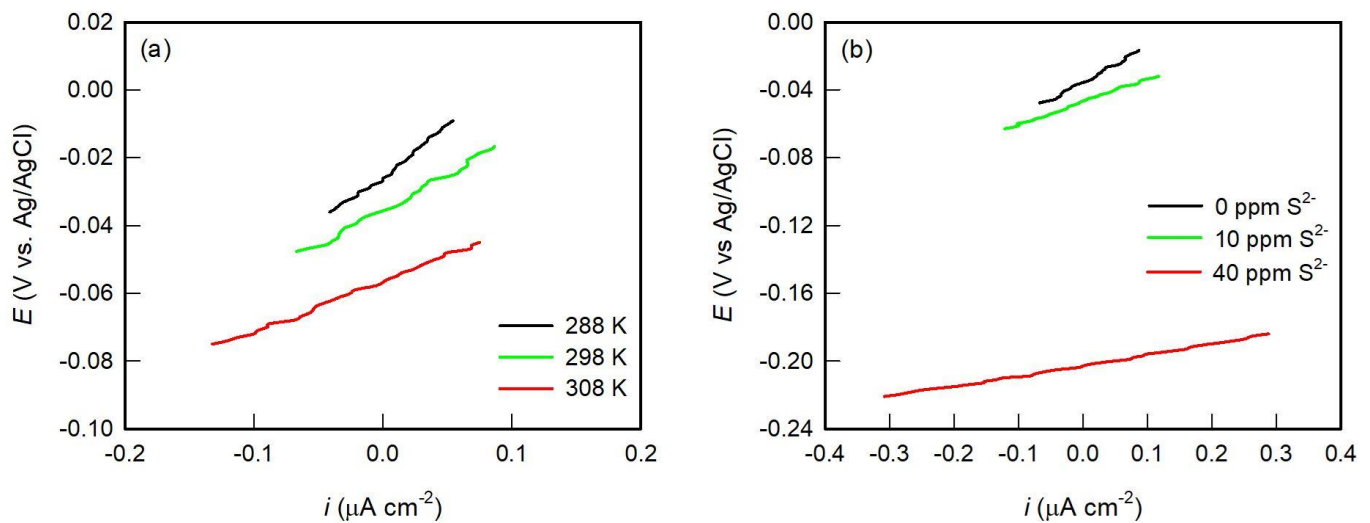
Figure 1. Open circuit potential curves for AISI 316L stainless steel in seawater at different (**a**) temperatures and (**b**) S^{2-} concentrations (at 298 K).

It can also be observed that the presence of S^{2-} ions (as seawater pollution) cause a significant shift of the potential toward more negative values (Figure 1b). Thus, it can be seen that an increase in concentration from 10 to 40 ppm of S^{2-} ions in seawater at 298 K shifts the E_{OC} up to 150 mV toward more negative values, from ≈ -60 mV to ≈ -200 mV.

Similar results are obtained for AISI 304L steel. With increasing seawater temperature in the range of 288–308 K, the final E_{OC} value decreases from -100 mV to -170 mV. The presence of sulfide ions also changes the E_{OC} value on the cathodic side from -120 mV (0 ppm S^{2-}, 298 K) to -310 mV (40 ppm, 298 K).

3.2. Electrochemical Impedance Spectroscopy Measurements

EIS is considered one of the least destructive and most informative techniques for characterizing electrochemical reactions at the metal/electrolyte interface and monitoring the interfacial phenomena of corrosion product film formation and modulation.

The results of EIS measurements for AISI 316L stainless steel in seawater under different experimental conditions (temperature, presence of S^{2-} ions) are shown in Figures 2 and 3. These results were further analyzed by fitting them with a suitable electrical equivalent circuit (EEC).

In the Nyquist complex plane, an incomplete capacitive semicircle is observed whose diameter decreases with increasing temperature (Figure 2a) and concentration of sulfide ions (Figure 3a). In the Bode complex plane (Figures 2b and 3b), the capacitive behavior of the studied systems is highlighted in a wide frequency range (at $f < 1$ kHz). The pronounced capacitive behavior is determined by a Bode line with a constant slope and phase angle with a broad peak and is the result of two overlapping time constants. This response indicates the formation of a surface film at the AISI 316L/seawater phase boundary.
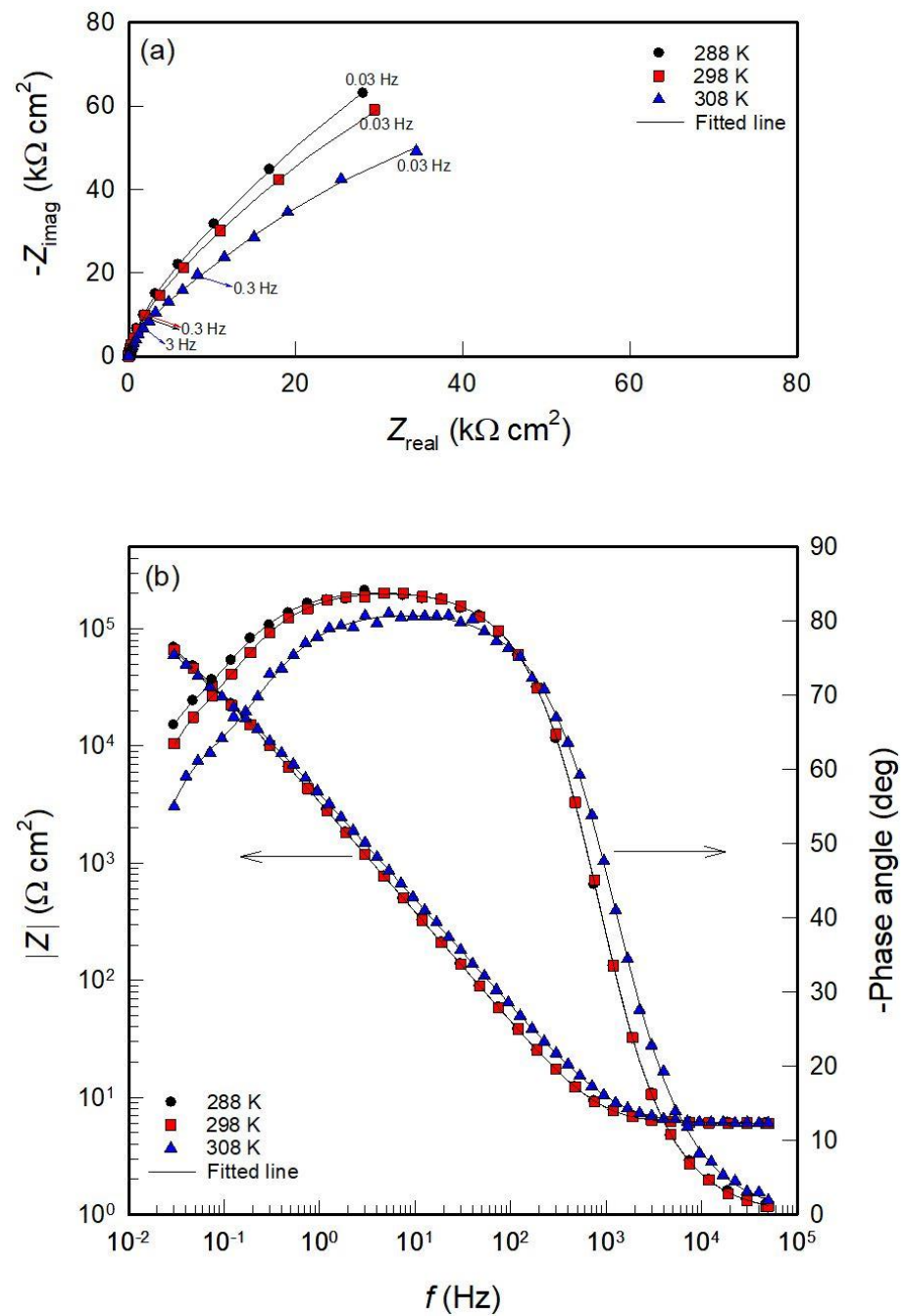
Figure 2. (**a**) Nyquist and (**b**) Bode diagrams for AISI 316L in seawater at different temperatures.
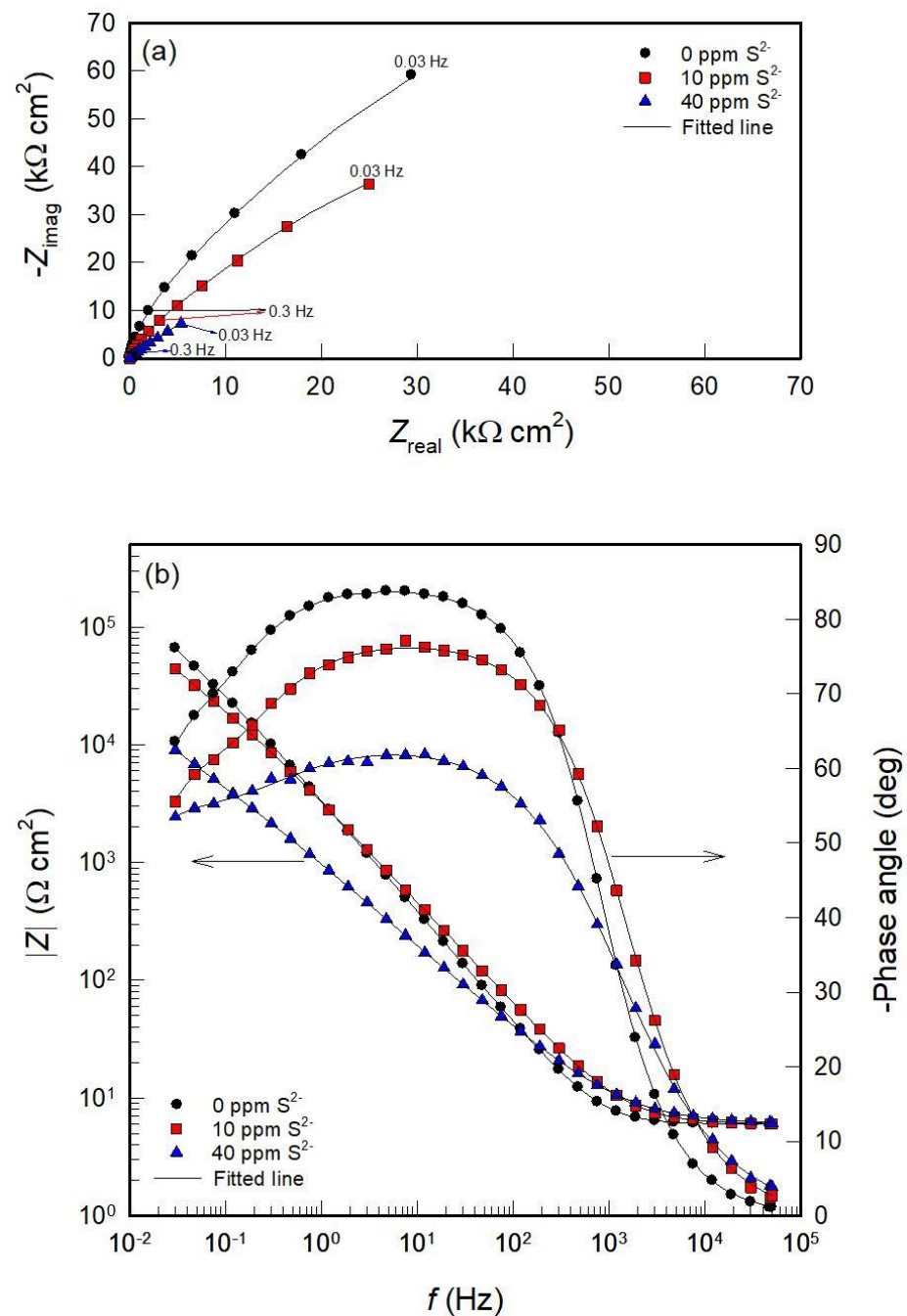
Figure 3. (**a**) Nyquist and (**b**) Bode diagrams for AISI 316L in seawater in the presence of S^{2-} ions at 298 K.

The total impedance of the phase boundary decreases with increasing temperature (Figure 2b) and concentration of sulfide ions (Figure 3b). A similar behavior is shown in the sample of AISI 304L steel, indicating that the protective properties of the surface film are lower under all experimental conditions. The obtained results are in agreement with the data in the literature [14,21,25,40–43]. When steel is exposed to seawater and neutral solutions containing inorganic chloride, sulfide, and sulfate-reducing bacteria, many authors have obtained similar impedance responses, and in analyzing the results, the equivalent electric circuit (EEC) model with two relaxation time constants is often used to represent a thin corrosion product film formed on the metal surface. Figure 4 shows the EEC model used to fit the EIS data.
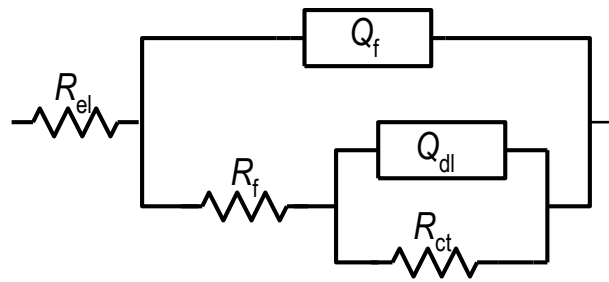
Figure 4. Electrical equivalent circuit (EEC) model used to fit the EIS data.

In the analysis of EIS results, the deviation of individual EEC elements from ideal behavior is described by the constant phase element (CPE), whose impedance, Z_{CPE}, is given by equation [44,45]:

$$Z_{CPE} = \left[Q(j\omega)^n\right]^{-1} \tag{1}$$

where ω is the angular frequency ($\omega = 2\pi f$), $j = \sqrt{-1}$, while Q is a combination of properties mainly related to the electrode surface. The CPE exponent n can take different values from -1 to $+1$ and accordingly replaces different elements in the EEC. The most common cases are when CPE represents the capacitance ($n = 1$) and the diffusion process ($n = 0.5$) [44,45].

In the proposed EEC, R_{el}, R_f, and R_{ct} are the electrolyte resistance ($\approx 6\ \Omega\ cm^2$), surface film resistance, and change transfer resistance, respectively. Q_f and Q_{ct} are the constant phase elements, which represent the capacitance of the surface film and electrochemical double layer, respectively, based on the corresponding parameter n. The calculated EEC parameters for the studied samples in seawater at different temperatures and concentrations of S^{2-} ions are shown in Table 4.

Table 4. Parameters of the equivalent circuit for AISI 304L and AISI 316L stainless steel in seawater at different temperatures and S^{2-} concentrations (at 298 K).

T (K)	$Q_f \times 10^6$ ($\Omega^{-1}\ s^n\ cm^{-2}$)	n_1	R_f (kΩ cm^2)	$Q_{dl} \times 10^6$ ($\Omega^{-1}s^n\ cm^{-2}$)	n_2	R_{ct} (kΩ cm^2)
			AISI 304L			
288	65.32	0.93	88.34	54.39	0.95	135.63
298	64.22	0.91	76.56	58.53	0.96	102.31
308	60.47	0.85	40.21	62.76	0.93	74.37
10 ppm S^{2-}	81.76	0.79	32.38	70.11	0.85	69.15
40 ppm S^{2-}	387.28	0.68	7.61	189.63	0.71	35.18
			AISI 316L			
288	53.41	0.94	113.57	40.28	0.95	182.85
298	53.05	0.94	89.61	43.33	0.95	140.76
308	47.11	0.91	57.34	49.17	0.94	102.04
10 ppm S^{2-}	62.15	0.86	47.36	55.53	0.89	95.01
40 ppm S^{2-}	270.48	0.71	13.71	140.72	0.75	47.78

The results obtained show that the experimental conditions (temperature and presence of S^{2-} ions) reduce the stability of the surface layer and favor the corrosion of the steel, which is more pronounced in the AISI 304L sample. The data in Table 4 confirm that the dynamics of the changes in EEC parameters (R_{ct}, R_f, Q_{ct}, and Q_f) are the same for both steel samples under different experimental conditions. Let us now consider the data for the AISI 316L sample.

The values of R_{ct} and R_f are high at 182.85 kΩ cm^2 and 113.57 kΩ cm^2, respectively, at 288 K, which is due to the formation of a stable and compact surface film. As the temperature increases, the resistances R_{ct} and R_f decrease significantly and are 102.04 kΩ cm^2 and 57.34 kΩ cm^2 at 308 K, respectively. This indicates that an increase in temperature has a strong effect on the thermodynamic stability of the oxide film. Apparently, the accelerated corrosion

rates associated with higher temperatures increasingly perturbed the interface, resulting in a less ordered, more porous, and less protective corrosion product layer [46,47].

The above changes lead to an increase in the rates of interfacial reactions that favor the corrosion of steel in seawater. This is confirmed by the fact that the thickness of the surface film (which is proportional to $1/Q_f$) increases slightly with temperature while the thickness of the double layer ($1/Q_{dl}$) decreases.

The presence of sulfide ions significantly increases the corrosion of steel in seawater (possibly due to the synergistic effect of the aggressive anions S^{2-} and Cl^-). Thus, the R_f value for AISI 316L in a 40 ppm sulfide-containing medium (at 298 K) is $\approx 14\,k\Omega\,cm^2$, which is 60% lower than the value in pure seawater, i.e., $\approx 90\,k\Omega\,cm^2$. The decrease in R_{ct} value is even more pronounced. R_{ct} in 40 ppm sulfide-containing seawater is $\approx 50\,k\Omega\,cm^2$ compared to $\approx 150\,k\Omega\,cm^2$ in pure seawater (so the decrease is more than 70%). On the other hand, Q_{dl} and Q_f increase dramatically while the corresponding parameters n_1 and n_2 decrease (i.e., the thickness and compactness of these films decrease).

The obtained results are consistent with the data in the literature, where many researchers have studied the effects of sulfide (including inorganic [13–15,21,48–54] and biogenic sulfide by SRB [15,39–42,54–57]) on the corrosion behavior of various stainless steels in seawater under different experimental conditions. EIS measurements show that small amounts of dissolved free sulfide (i.e., H_2S, Na_2S, HS^-, and S^{2-}) cause a significant decrease in the overall resistance and an increase in the capacity of stainless steels [14,15,41,49–53,58]. Moreover, sulfides cause similar behavior in other media (cooling water, hydrocarbons). For example, Ge et al. indicate that the addition of sulfide (up to 9 mM) to simulated cooling water causes a rapid reduction in impedance. The film resistance decreases from 13.01 to 0.30 $M\Omega\,cm^2$ within 1 h [50].

These results are attributed to the detrimental effect of sulfide ions on the integrity and protective properties of the corrosion product film due to the transformation of iron oxides to iron sulfides [15,39–41,48,51,54–57]. In other words, the sulfidation of the passive film leads to a decrease in the R_f value, and the faster the sulfidation process proceeds, the lower the resistance of the passive film.

3.3. Polarization Measurements

After stabilizing the stainless steels in seawater (at different conditions), the polarization resistance R_p was determined using the linear polarization resistance (LPR) method. Since the potential disturbance in this method is very small (only ± 20 mV around the E_{OC}), LPR is essentially a nondestructive method, which is the main advantage over other DC corrosion measurement methods. The results of the LPR measurements for AISI 316L are shown in Figure 5.
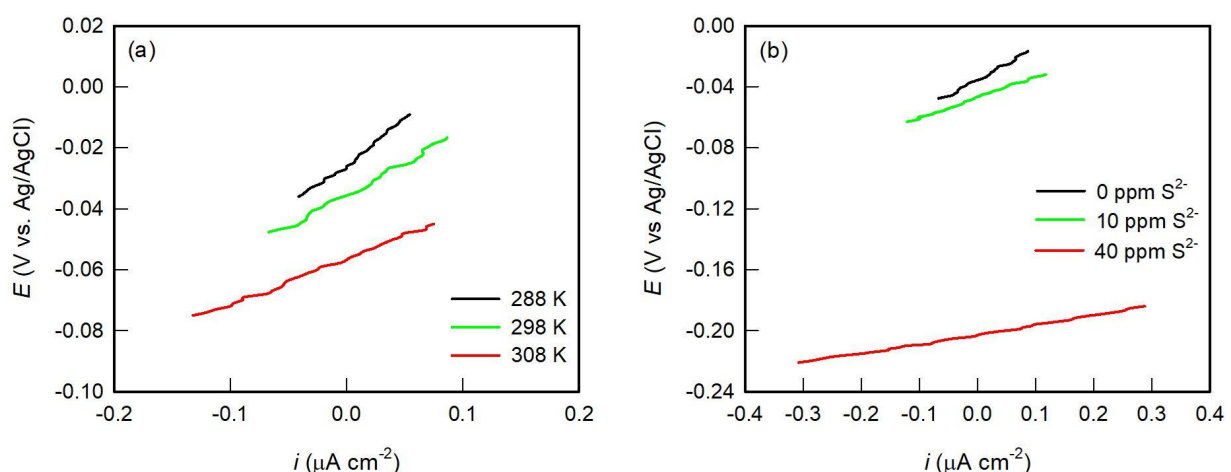
Figure 5. Linear parts of polarization curves for AISI 316L stainless steel in seawater at different (**a**) temperatures and (**b**) S^{2-} concentrations (at 298 K).

As can be seen, a linear relationship between the applied potential and the current response (linear *i-E* dependence) was obtained in all measurements. Depending on the experimental conditions, i.e., the temperature of the fresh seawater as well as the presence of S^{2-} ions in the seawater, the slope of the linear dependencies changes. The *i-E* slope defines the polarization resistance of the tested system, R_p:

$$R_P = \frac{\Delta E}{\Delta i} \tag{2}$$

A decrease in the *i-E* slope corresponds to a decrease in the value of R_p (Table 5). Since this is consistent with the Stern–Geary equation, the corrosion current i_{corr} is inversely proportional to the polarization resistance [58]:

$$i_{corr} = \frac{b_a b_c}{2.303(b_a + b_c)} \frac{1}{R_p} = \frac{B}{R_p} \tag{3}$$

Table 5. Corrosion parameters for the stainless steels AISI 304L and AISI 316L in seawater at different temperatures and different Na$_2$S concentrations (at 298 K).

T (K)	E_{corr} (V)	i_{corr} (μA cm^{-2})	i_p (μA cm^{-2})	E_{dp} (V)	$E_{dp} - E_{corr}$ (V)	R_p (kΩ cm^2)	v_{corr} (mm y^{-1})
			AISI 304L				
288	−0.18	1.89	3.27	0.40	0.58	212.79	0.0195
298	−0.18	2.56	7.84	0.34	0.52	167.15	0.0265
308	−0.20	3.36	13.94	0.24	0.44	116.05	0.0347
10 ppm S^{2-}	−0.23	3.95	14.35	0.30	0.53	101.99	0.0408
40 ppm S^{2-}	−0.28	5.85	31.53	0.21	0.49	46.38	0.0605
			AISI 316L				
288	−0.11	0.95	1.89	0.57	0.68	284.24	0.0099
298	−0.12	1.26	4.10	0.48	0.60	209.32	0.0132
308	−0.13	1.86	7.53	0.42	0.55	149.82	0.0194
10 ppm S^{2-}	−0.18	2.24	9.21	0.34	0.52	145.84	0.0234
40 ppm S^{2-}	−0.23	3.20	19.57	0.28	0.51	62.65	0.0334

A decrease in polarization resistance indicates an acceleration of corrosion rate and vice versa (b_a and b_c are the anodic and cathodic Tafel slopes, respectively). An increase in seawater temperature and contaminant concentration adversely affects the corrosion stability of AISI 304L and AISI 316L stainless steel. Similar results were obtained for both steel samples. Table 4 shows that R_p decreases twofold with increasing temperature and fourfold with increasing sulfide ion concentration.

The general corrosion behavior of AISI 304L and AISI 316L steels in seawater at different conditions was investigated by recording the potentiodynamic polarization curves (PD) over a wide potential range. Figure 6 shows the results for AISI 316L steel in seawater at different temperatures and concentrations of S^{2-} ions. The corresponding polarization parameters are listed in Table 5. Both stainless steel samples show similar polarization behavior. Since inert gas did not flow through the solution and the cell was not hermetically sealed, the cathodic branch of the polarization curve most likely describes the reduction in water and dissolved oxygen.
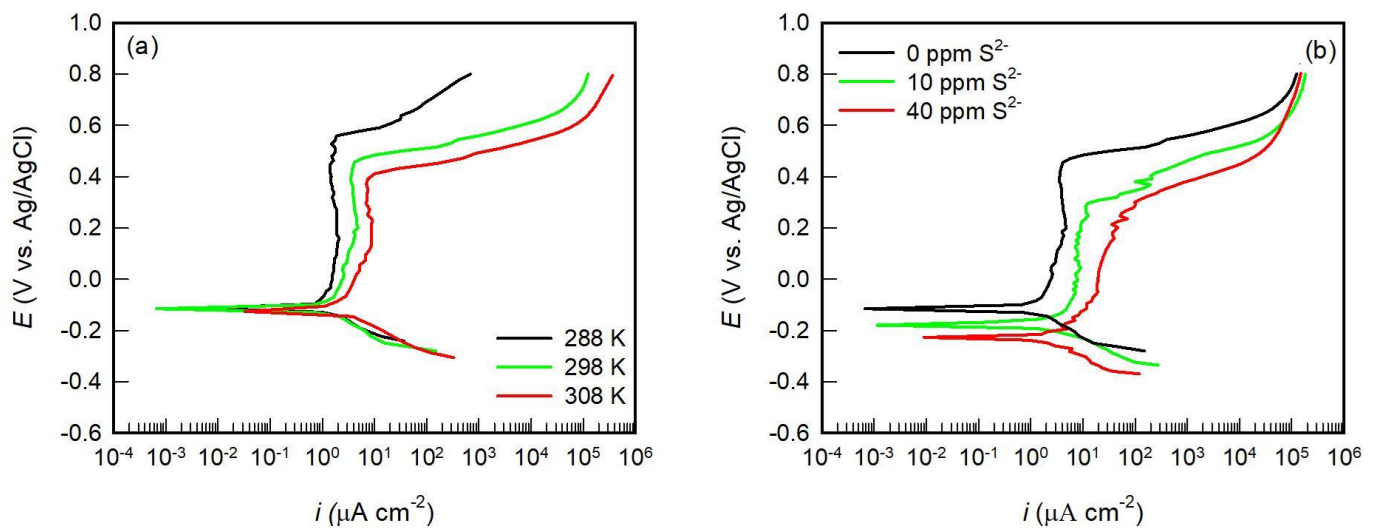
Figure 6. Potentiodynamic polarization curves for AISI 316L stainless steel in seawater at different (**a**) temperatures and (**b**) S^{2-} concentrations (at 298 K).

A potentiodynamic polarization curve is usually presented in a semi-logarithmic diagram and consists of cathodic and anodic curves, which are the result of electrochemical reactions in the system. The polarization curves in Figure 6 show clear evidence of an active–passive transition, as expected for stainless steels in seawater environments. Accordingly, three potential regions can be observed on the anodic branch of the polarization curves (potentials more positive than E_{corr}): active, passive, and metal depassivation regions. In the active potential region, the steel samples dissolve and release metal ions to the seawater, and the current increases exponentially with increasing potential (i.e., a linear relationship log *i*-*E* is observed on the PD curve). In seawater, the metal ions come into contact with the OH^- ions (formed by the ionization of water) and form hydroxides that cover the steel surface, which further slows down the metal dissolution. During dehydration, the metal hydroxide transforms into the corresponding oxide.

During further anodic polarization, the rate of dissolution of the metal becomes equal to the rate of oxide film formation, and a passivation current (i_p) is established. By further increasing the potential, the rate of the dissolution of the metal significantly slows down the process of oxide film formation. Eventually, the entire surface of the metal is covered with a passive film, and a more or less defined "current plateau" forms on the PD curve. The "current plateau" (the independence of the current from the potential in the potentiodynamic conditions of the experiment) is associated with the growth (thickening) of the passive film by ionic conductivity, which involves a transport process driven by the electric field in the oxide layer [59].

The starting point for the analysis of the PD curves is the corrosion potential (E_{corr}) and its corresponding corrosion current density (i_{corr}). With increasing temperature, the E_{corr} of both steels shifts very slightly into the negative range, while the i_{corr} increases (Table 5). Although the influence of the temperature increase (from 288 to 308 K) on the E_{corr} shift is almost insignificant ($\approx$20 mV), the i_{corr} actually increases twice (from 1.89 to 3.36 μA cm^{-2} for AISI 304L and from 0.95 to 1.86 μA cm^{-2} for AISI 316L). Increasing the temperature from 288 to 308 K resulted in a significant increase in current densities in the active anodic and passive regions, while the cathodic effect was not very pronounced. In addition, higher temperatures did not have a pronounced effect on the corrosion potentials but significantly lowered the primary passive potentials, decreased the passive potential range, and reduced the pitting potentials. All these results (Table 5) clearly show that temperature adversely affects the corrosion behavior of AISI 304L and AISI 316L stainless steels, which is consistent with the data in the literature for seawater and other aggressive environments [31,32,46–49,60,61]. The temperature was found to affect pitting potential

values more than chloride concentration. Moreover, an increase in temperature up to 90 °C in Cl^- ion-containing electrolytes decreased the pitting potential by more than 200 mV [31,61].

In the active potential range, the presence of S^{2-} ions (up to 40 ppm) shifted E_{corr} by $\approx$100 mV on the active (cathodic) side for both samples and increased the i_{corr} more than twice (from 2.56 to 5.85 μA cm^{-2} for AISI 304L and from 1.26 to 3.20 μA cm^{-2} for AISI 316L). Moreover, in the passive potential region, the presence of S^{2-} ions increased the current densities in the passive and transpassive regions and significantly lowered the primary passive potentials, the passive potential region, and the pitting potentials, which were observed with increasing temperature. This suggests that the presence of S^{2-} ions negatively affects the corrosion behavior of stainless steels in saltwater environments.

As already mentioned, this effect was observed in the presence of inorganic sulfide [13–15,48–54] and in the presence of biogenic sulfide (known in the literature as SRB) [15,39–41,52,54–57] in various media (seawater, artificial seawater, aggressive environments with Cl^- ions, then in artificial wastewater, in the oil industry, etc.).

In investigating the corrosion behavior of AISI 304L steel, Yuan et al. found that the E_{corr} of specimens in artificial seawater remains fairly constant (about -0.17 V), while i_{corr}, after 42 days of exposure, shows a slight decrease (from 3.9 to 3.2 μA cm^{-2}) due to the formation of conditioning layers and passive oxide layers. However, under the influence of inorganic sulfide ions, E_{corr} experiences a negative shift of about 100 mV (-0.28 V), while i_{corr} is about twice as large (about 8.3 μA cm^{-2}) [15]. The increased corrosion rate of stainless steels is mainly due to the accelerated conversion of metal oxides to metal sulfides by the inorganic sulfide, which has been confirmed by various surface analysis techniques [15,48,51,54]. However, the conversion of metal oxides to metal sulfides by inorganic sulfide is slower than by biogenic sulfide (in the presence of active SRB) [15,54]. In the literature, organic sulfides and corrosive sulfide intermediates have been found to be involved in the sulfurization process using biogenic sulfides [15,40,41,54–57]. Despite extensive research, the mechanism of the complex action of biogenic sulfides is still not fully understood.

The results for AISI 316L show that in the temperature range 288 to 308 K, the passivation current rises from $\approx$2 to $\approx$7.5 μA cm^{-2}, while the addition of 10 ppm sulfide causes an increase in i_p from $\approx$4 to $\approx$9 μA cm^{-2} (Table 5). When 40 ppm of sulfide is added, i_p increases to $\approx$20 μA cm^{-2}, which is about five times higher than the i_p value in the system free of sulfide. When testing 316L stainless steel in simulated cooling water containing various sulfide concentrations, a significant increase in i_p was also observed (an increase in sulfide ion concentration up to 9 mM increases i_p twofold, from $\approx$13 to $\approx$24 μA cm^{-2}) [50]. Namely, in a sense, i_p reflects the rate of penetration of corrodent through the passive film. Its increase indicates the deterioration of the protective performance of the passive film and illustrates that the sulfide has changed the performance of the passive film. Marcus [62] suggested that sulfide can weaken the binding energy of the metal–metal bonds on the surface, leading to an increase in the anodic dissolution rate of the metal. That is, the presence of sulfide lowers the activation energy of the metal dissolution reaction and accelerates the anodic dissolution process of the metal. Moreover, as mentioned earlier, the addition of sulfide leads to a significant reduction in corrosion potential. Further polarization leads to the pitting or depassivation potential (E_{dp}), which becomes more negative with increasing temperature and seawater pollution (i.e., the presence of S^{2-} ions) in the steel specimens studied (Table 5). At the E_{dp}, degradation of the passive layer and local metal dissolution occurs, which is accompanied by a sudden increase in the anodic current.

Since the E_{corr} value of the steels studied depends on the experimental conditions (Table 5), the range of passive potential is more precisely determined by the potential difference, given as $\Delta E = E_{dp} - E_{corr}$, which decreases for both samples with increasing temperature and sulfide ion concentration. In agreement with the literature, the potential difference $E_{dp} - E_{corr}$ (denoted as ΔE, representing the range of passive potentials) is indicative of the pitting initiation rate; the higher it is, the slower the pitting initiation rate [63,64].

Table 5 contains the values of the corrosion rate v_{corr} (expressed in millimeters per year; mm/y) calculated using the following equation:

$$v_{corr} = \frac{i_{corr}M}{\rho F z} \tag{4}$$

where M is the molar mass of the corroding species, ρ is the density of the corroding species, F is the Faraday constant, and z is the electron number. In calculating the corrosion rate, the data for ρ, M, and z were determined based on the percentage of the main elements in AISI 304L (Fe and Cr) and AISI 316L (Fe, Cr, Mo) steel [65]. The corrosion rate of both steels increased with increasing temperature and concentration of sulfide ions, with the AISI 316L steel exhibiting a lower corrosion rate. The literature data for v_{corr} vary considerably. For example, Adebayo et al. recorded as much as ten times higher values for v_{corr} (≈ 0.72 mm y^{-1}) in chloride solutions saturated with H_2S at 298 K [53], which is probably a consequence of a higher concentration of S^{2-} ions, while Malik et al. found as much as ten times lower values (≈ 0.005 mm y^{-1}) [60] (which is a consequence of the much lower concentration of Cl^- ions compared to the conditions in this work; seawater).

3.4. Surface Analysis

After impedance measurements (at E_{OC}) and after anodic polarization measurements (which ended at 0.8 V) in seawater at 298 K, the steel surfaces were examined by SEM/EDS analysis, and the results obtained are shown in Figure 7 and Table 6. It should be emphasized that corrosion products were not removed from the surface of the samples after the electrochemical measurements.
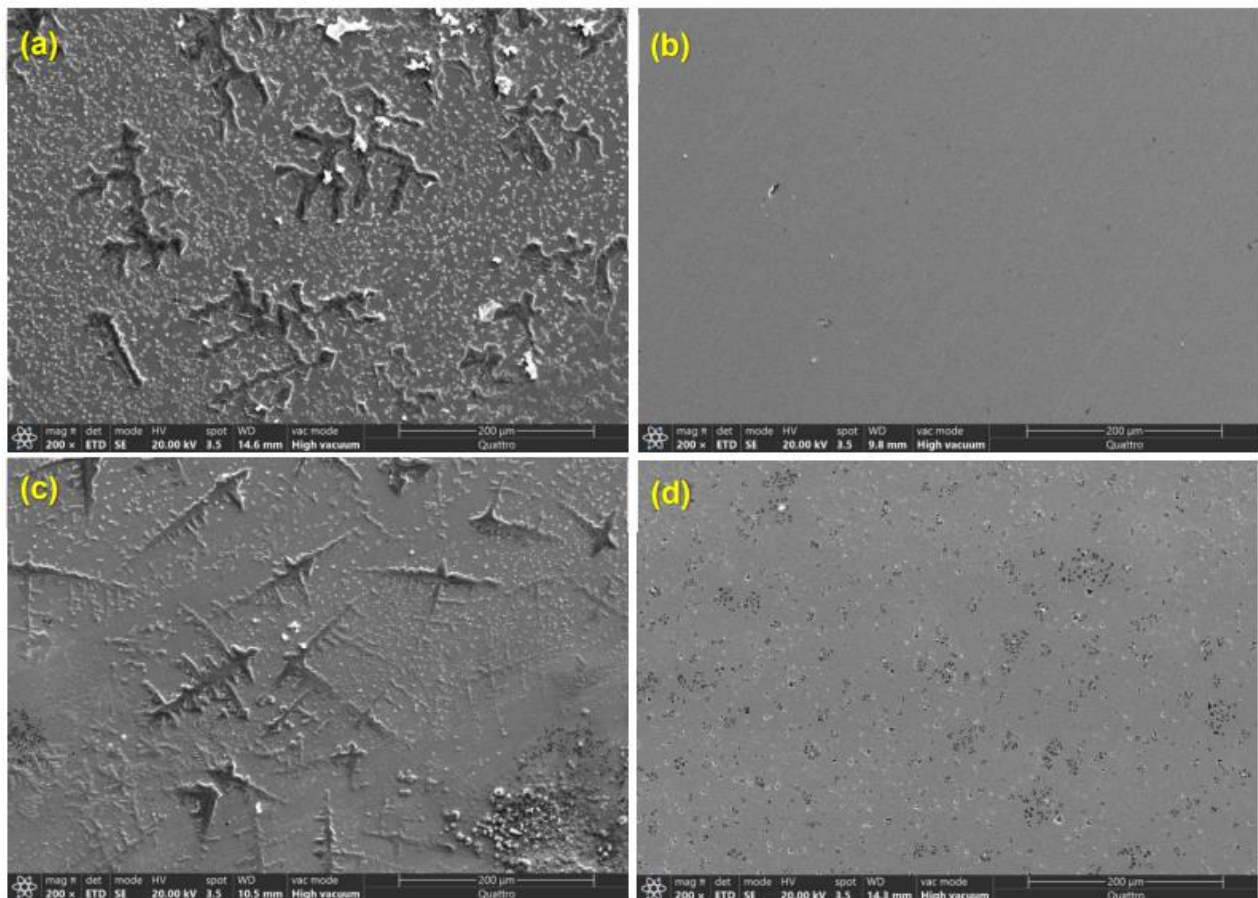
Figure 7. SEM image after impedance measurements for (**a**) AISI 304L and (**b**) AISI 316L and after anodic polarization measurements for (**c**) AISI 304L and (**d**) AISI 316L in seawater at 298 K.

Table 6. Average elemental composition of the entire surface for AISI 304L and AISI 316L after impedance (EIS) and potentiodynamic polarization (PD) measurements in seawater at 298 K.

| Element (wt.%)	AISI 304L		AISI 316L	
	EIS	PD	EIS	PD
O	2.80	2.38	5.79	4.33
Na	15.08	11.34	-	1.85
Mg	1.38	1.05	-	0.45
Si	0.42	0.34	0.04	0.44
Cl	7.14	5.04	0.07	1.10
Cr	13.77	14.78	16.36	16.42
Mn	0.99	1.15	1.11	1.00
Fe	52.67	57.50	67.91	64.91
Ni	5.75	6.02	7.43	7.25
Mo	-	-	1.92	2.25
K	-	0.19	-	-
Ca	-	0.21	-	-
Total	100.00	100.00	100.00	100.00

Exposure of AISI 304L to seawater results in damage to most of the surface, which is covered with coarse deposits of corrosion products and NaCl (according to EDS analysis). In contrast, under the same conditions, the surface layer of AISI 316L is smooth and even and shows almost no signs of the corrosion process. It should be noted that anodic polarisation produces a rough surface morphology of corrosion products over the damaged AISI 304L steel. On the AISI 316L specimen, there are several small damages, such as pits, covered by a fine layer of corrosion products.

EDS analysis of total surface area AISI 304L and AISI 316L steels in seawater under EIS and PD measurements show the presence of Fe, Cr, Mn, Ni, and Si (as the main alloying elements), then the presence of Na, Mg, Cl, K, Ca, and O (as constituents of seawater). The presence of oxygen indicates that the surfaces of both samples are covered with a protective oxide layer. Compared to AISI 304L, a higher O content and an almost negligible percentage of Na and Cl were found on the surface of AISI 316L, while the other elements were consistent with the original composition of the alloy (Table 1). This additionally confirms the fact that the oxide layer on the AISI 316L sample is more resistant to chloride adsorption and ingress and has a better corrosion property. Indeed, the highly perturbed surface of the AISI 304L can be related to the high chloride affinity of the oxide layer.

In the literature, the general opinion is that the surface oxide layer on stainless steel is very thin (order of a few nm [66–70]) and consists mainly of a mixture of iron and chromium oxides/hydroxides, and in some cases, also contains small amounts of molybdenum oxide [68–70].

Results of electrochemical measurements are attributed to the detrimental effect of sulfide ions on the integrity and protective properties of the corrosion product film due to the transformation of iron oxides into iron sulfides [15,39–41,48,51,54–57]. This statement is confirmed by the SEM/EDS analysis performed on both steel samples under different experimental conditions in seawater with 40 ppm S^{2-} ions at 298 K. The obtained results are shown in Figures 8 and 9 and Tables 7 and 8 (the layers of corrosion product were not removed from the surface of the sample product).
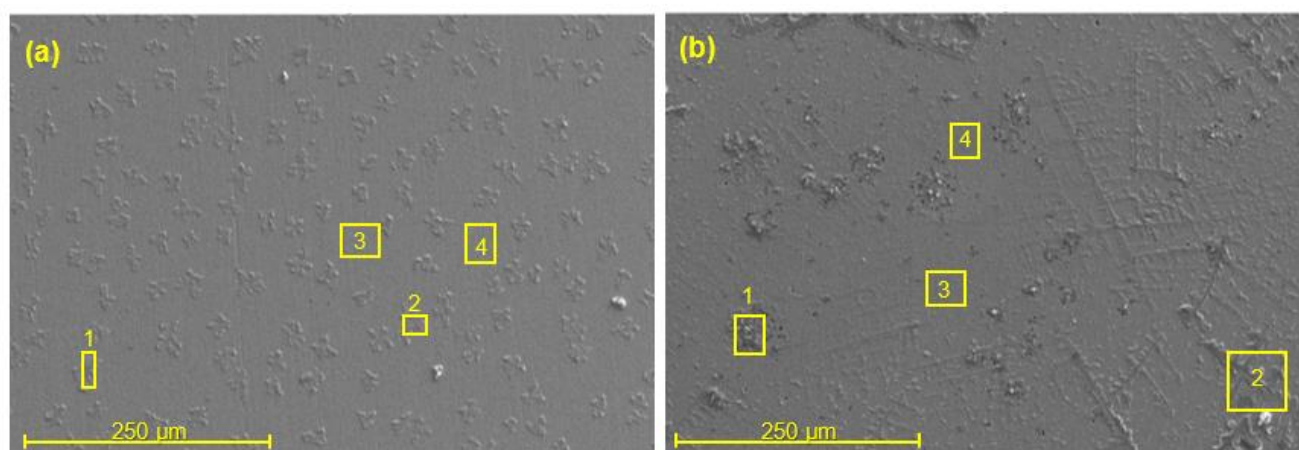
Figure 8. SEM image after impedance measurements for (**a**) AISI 304L and (**b**) AISI 316L in seawater with 40 ppm S^{2-} ions at 298 K with marked parts of EDS analysis (yellow numbers).
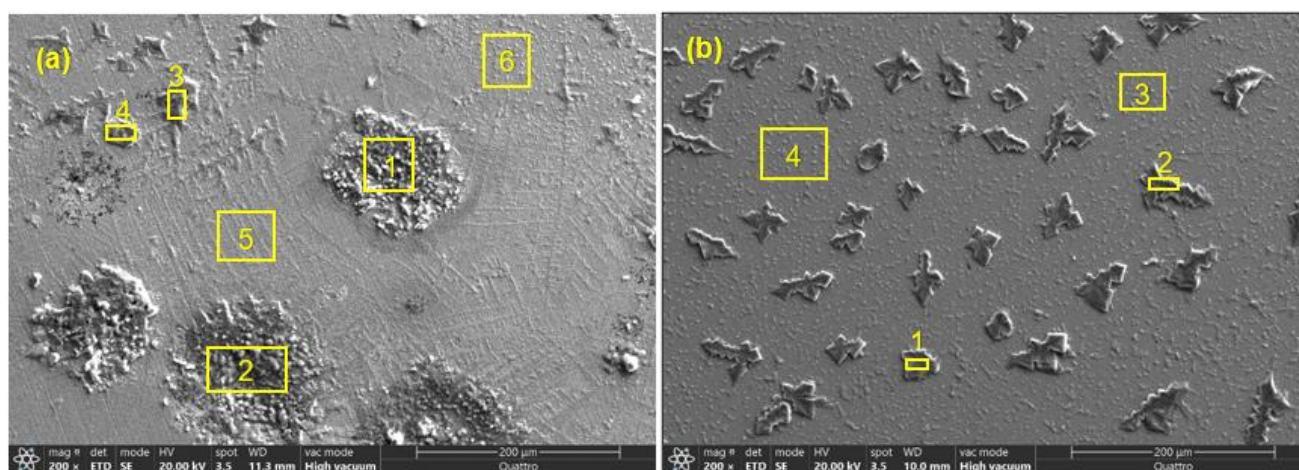
Figure 9. SEM image after potentiodynamic polarization measurements for (**a**) AISI 304L and (**b**) AISI 316L in seawater with 40 ppm S^{2-} ions at 298 K with marked parts of EDS analysis (yellow numbers).

Table 7. Elemental composition on marked parts of the surface of AISI 304L and AISI 316L steels after impedance measurements in seawater with 40 ppm S^{2-} ions at 298 K.

	AISI 304L				AISI 316L			
Element (wt.%)	1	2	3	4	1	2	3	4
O	1.90	1.06	0.87	1.88	8.73	3.65	2.76	2.71
Na	13.31	15.67	2.14	2.05	20.21	20.53	1.28	4.53
Mg	1.36	0.55	-	-	3.67	1.29	1.17	-
Si	0.40	0.38	0.47	0.47	0.14	0.27	0.32	0.34
S	0.25	0.28	0.08	0.08	3.27	0.66	0.62	0.51
Cl	5.46	5.73	0.70	0.62	18.16	9.97	0.60	1.70
Cr	15.04	14.63	17.84	17.65	8.53	12.77	17.05	16.06
Mn	0.97	1.38	1.25	1.41	0.69	1.72	1.23	1.28
Fe	56.91	54.33	68.50	68.16	30.44	42.45	64.60	61.76
Ni	5.76	5.99	8.15	7.68	4.06	5.77	8.71	8.71
Mo	-	-	-	-	0.75	0.76	1.66	2.40
K	-	-	-	-	0.65	0.16	-	-
Ca	.	-	-	-	0.70	-	-	-
Total	100.00	100.00	100.00	100.00	100.00	100.00	100.00	100.00

Table 8. Elemental composition on marked parts of the surface of ALSI 304L and AISI 316L steels after potentiodynamic polarization measurements in seawater with 40 ppm S^{2-} ions at 298 K.

| Element (wt.%)	AISI 304L						AISI 316L			
	1	2	3	4	5	6	1	2	3	4
O	0.58	0.65	0.77	0.63	2.65	2.36	1.69	2.45	3.15	3.36
Na	28.69	28.75	29.87	36.11	6.67	5.78	34.71	34.92	4.96	3.26
Mg	0.88	0.98	0.71	-	1.22	0.77	0.43	1.72	-	-
Si	-	0.16	0.17	-	0.41	0.51	-	-	0.30	0.30
S	3.41	3.70	2.45	2.04	0.69	0.35	0.26	0.54	0.05	0.07
Cl	38.83	47.98	44.25	37.22	2.29	1.93	25.76	38.75	1.60	1.18
Cr	4.06	4.70	4.20	4.99	16.05	16.76	7.14	4.38	16.55	16.50
Mn	0.62	0.55	0.32	0.51	1.27	1.04	0.38	-	1.05	1.41
Fe	12.00	9.82	15.67	16.69	62.30	63.72	24.74	14.81	63.63	64.88
Ni	1.41	0.87	1.36	1.80	6.46	6.78	3.60	1.94	7.01	7.21
Mo	-	-	-	-	-	-	0.74	0.30	1.68	1.84
K	-	0.39	-	-	-	-	0.38	0.41	-	-
Ca	1.52	1.46	0.23	-	-	-	0.19	0.29	-	-
Total	100.00	100.00	100.00	100.00	100.00	100.00	100.00	100.00	100.00	100.00

Compared to pure seawater (Figure 7), the surface of both samples in the presence of sulfide ions exhibits a rougher morphology, with individual steel areas covered with higher quantities of corrosion products. These changes are particularly pronounced after polarization measurements on a sample of AISI 304L steel.

EDS analysis of the different parts of the AISI 304L and AISI 316L surface after EIS and PD measurements (positions 1–6) shows significant changes in the elemental composition, especially in Fe, Cr, and other basic elements of the alloy, the content of which has decreased significantly due to the dissolution. In parallel with these changes, a decrease in O content and an increase in S content were observed. The changes on the surface are again greatest for the AISI 304L sample after the measurements of PD. To determine the condition of the surface under the corrosion products after the potentiodynamic polarization measurements, the layers of corrosion products were removed from the steel specimens with ultrasonic cleaning in deionized water. The occurrence of pitting corrosion (density, depth, and width of pits) on the surface of the samples was confirmed with optical microscopy and a non-contact 3D profilometer. The light microscopy results are shown in Figures 10 and 11.

The pits on the surfaces of both types of stainless steel can be clearly seen in these figures. It should be noted that the AISI 304L steel has larger pits at the same seawater temperature, confirming that the AISI 304L stainless steel is more susceptible to pitting corrosion compared to the AISI 316L steel.

The introduction of sulfide ions into seawater leads to a change in the shape and size of the pits and their size, which become larger in AISI 304L stainless steel (Figure 11a), while in AISI 316L, the number of pits on the alloy surface increases (Figure 11b).

More accurate information about the surface topography was obtained by profilometric measurements, as shown in Figure 12. The technique of non-contact 3D profilometer analysis provides an ideal, user-friendly way to maximize surface examination when pitting analysis is required, along with the advantages of combined 2D and 3D capability [71].
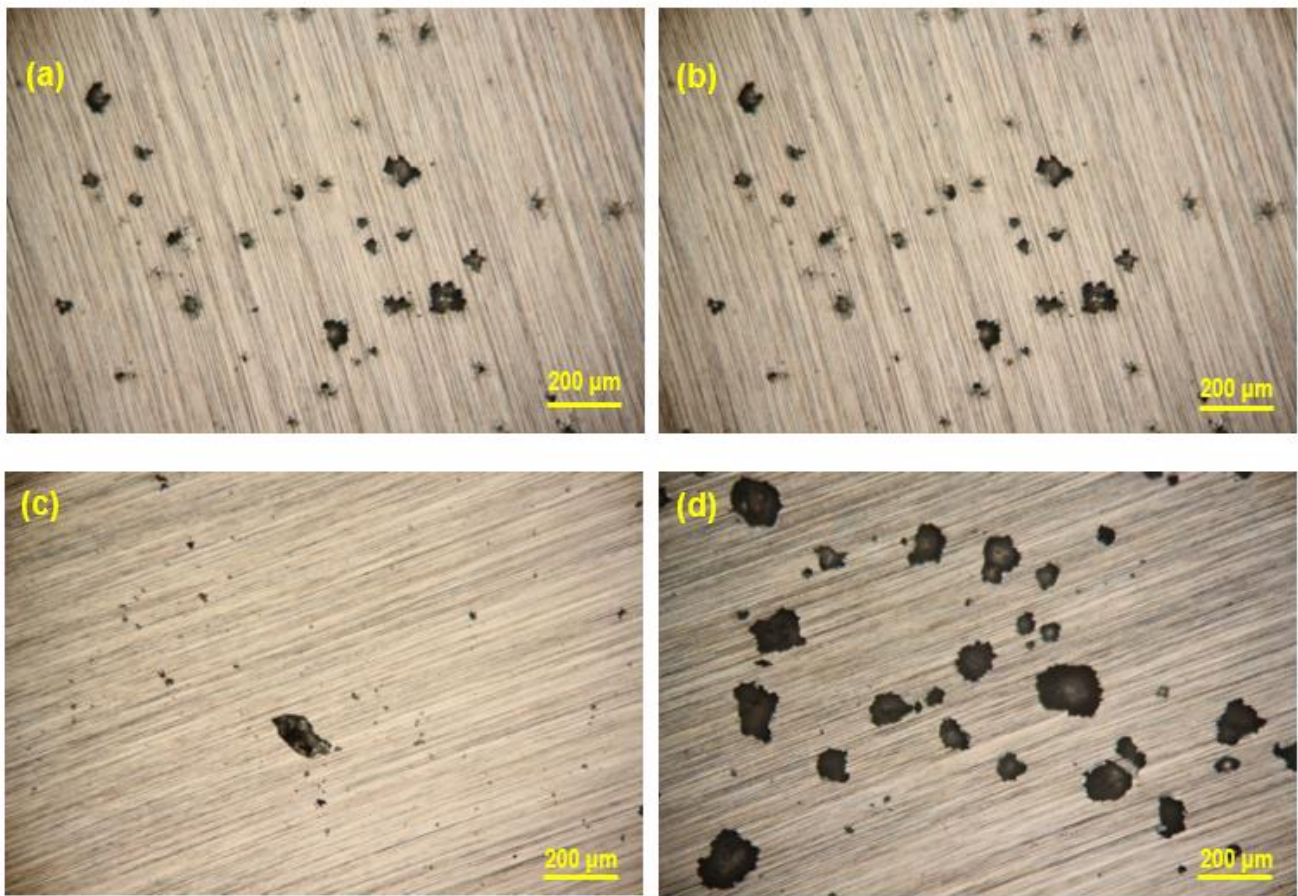
Figure 10. Optical micrographs for AISI 304L after potentiodynamic polarization measurements in seawater at (**a**) 288 K and (**b**) 308 K and for AISI 316L at (**c**) 288 K and (**d**) 308 K (100× magnification).
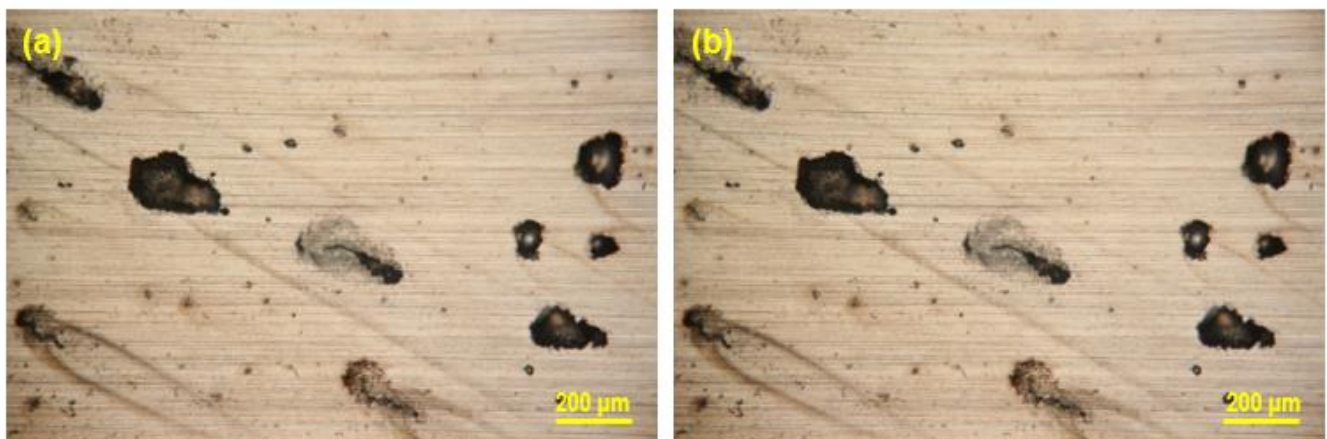
Figure 11. Optical micrographs after potentiodynamic polarization measurements in seawater at 298 K in the presence of 10 ppm of S^{2-} for (**a**) AISI 304L and (**b**) AISI 316L (100× magnification).
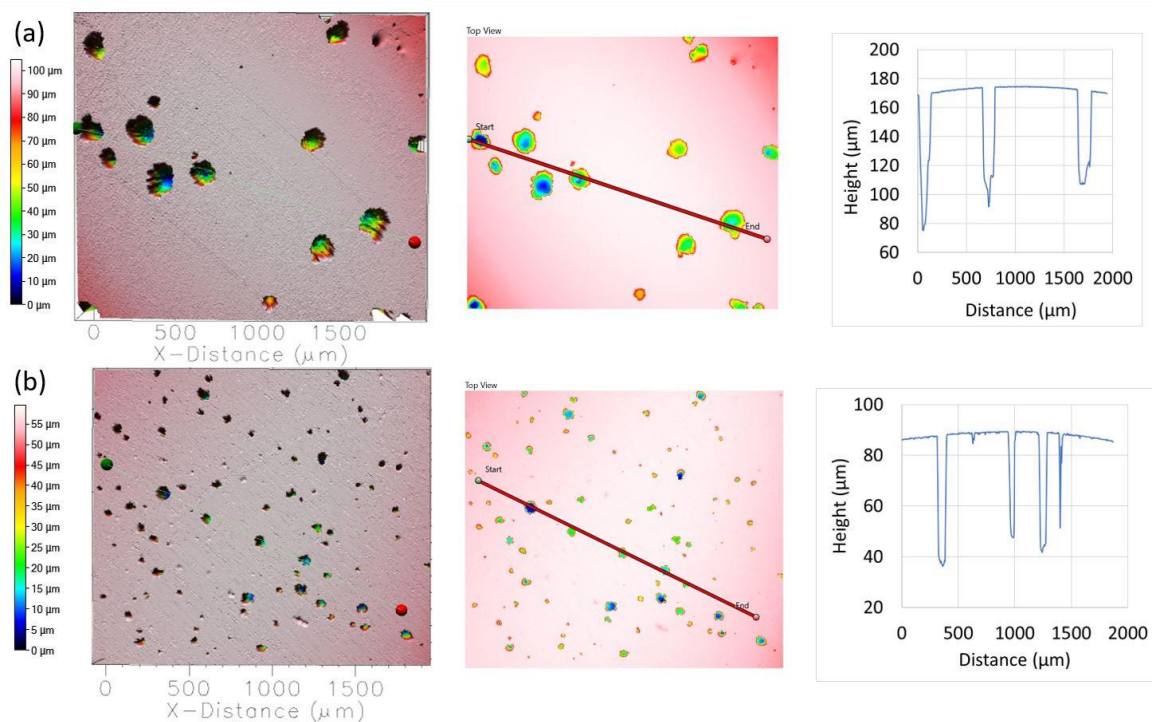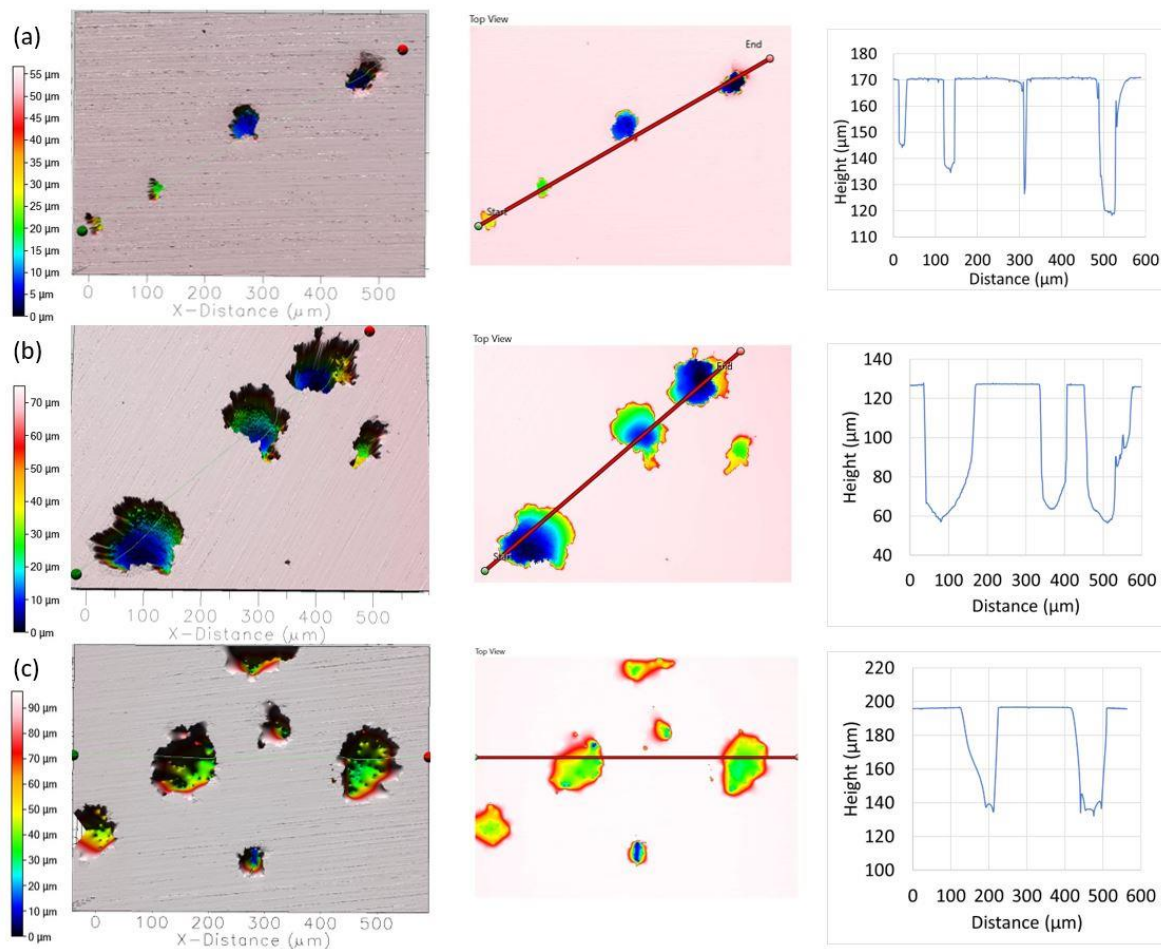
Figure 12. Topographic view of the segment of corroded surfaces in seawater at 298 K after potentio-dynamic polarization measurement for (**a**) AISI 304L and (**b**) AISI 316L. The depth and width of pits are determined along the red lines.

The size, shape, and density of the pits were strongly affected by the type of stainless steel studied and the experimental conditions, e.g., seawater temperature and S^{2-} ion concentrations. Anodic polarization of AISI 304L steel led to the development of a few pits with an average depth of 80–100 μm and width of about 100 μm (Figure 12a). Under the same conditions, on the surface of AISI 316L steel, the number and density of pits increased, but their depth and width decreased. As shown in Figure 12b, pits with an average depth of 40–50 μm and a width of 50 μm are formed on the surface of AISI 316L steel.

The effect of seawater temperature on pit size is shown in Figure 13 for AISI 304L stainless steel. At 288 K, the scanned pit has a diameter of 10–25 μm and a maximum depth of 50 μm (Figure 13a). The situation worsens with increasing temperature, and at 298 K (Figure 13b), the depth and width of the pit increase to 70 μm and 100 μm, respectively. The situation was the worst at 308 K (Figure 13c), where the pit width and depth remained the same as at 298 K, but the number of pits on the surface increased. In general, it can be said that an increase in temperature does not affect the depth of the pits (at all temperatures, pits have a depth of about 50–70 μm). However, the number of pits as well as their width, increase significantly (for example, at a temperature increase from 288 to 308 K, the width of the pit increases fourfold, from 25 to 100 μm).
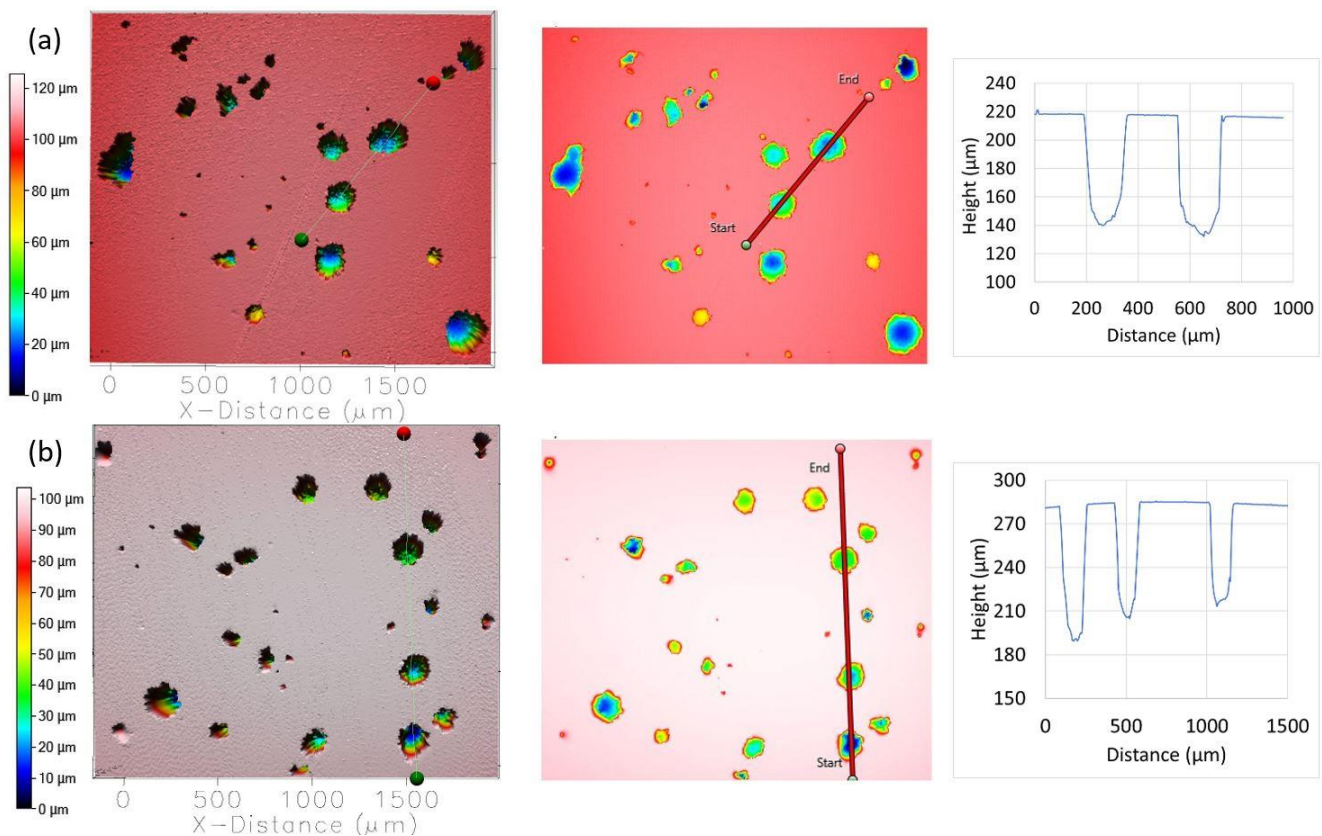
Figure 13. Topographic view of the segment of the corroded AISI 304L surface after potentiodynamic polarization measurement in seawater at (**a**) 288 K, (**b**) 298 K, and (**c**) 308 K. The depth and width of pits are determined along the red lines.

Figure 14 shows the analysis of pitting damage on the steel surfaces of AISI 304L after the potentiodynamic polarization method in polluted seawater with 10 ppm and 40 ppm of S^{2-} ions. The presence of sulfide at a concentration of only 10 ppm leads to the formation of pits with a depth of about 90 μm and a diameter of up to 200 μm, which is almost twice as large as the dimensions without S^{2-} ions. When the sulfide ion concentration is further increased, the size of the pits does not change, but their number increases slightly.

The deterioration of corrosion resistance of stainless steel exposed to polluted seawater can be explained by the mechanism described in the literature [13,21,71,72]. The proposed mechanism involves the adsorption of S^{2-} ions on the surface, which prevent the growth of the passivation film and increase its defectiveness. In this way, the adsorbed sulfide interacts with cations in the passive film on the surface and leads to the formation of sulfur-containing second phases, which results in an increase in the defect concentration of this layer (VM″) and, consequently, its ionic conductivity and ionic current density through the oxide [14,21,71,72]:

$$M_M'' + HS_{ads}^- \rightarrow MHS_{ads}^+ + V_M'' \tag{5}$$

$$MHS_{ads}^+ \rightarrow MS_{1-x} + xHS^- + (1-x)H^+ \tag{6}$$
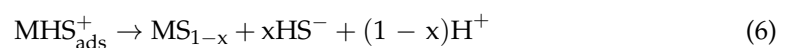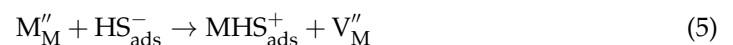
Figure 14. Topographic view of the segment of the corroded AISI 304L surface after potentiodynamic polarization measurement in seawater at 298 K with (**a**) 10 ppm of S^{2-} and (**b**) 40 ppm of S^{2-}. The depth and width of pits are determined along the red lines.

Moreover, the reaction described above leads to local acidification and, thus, to an increase in the dissolution rate of the passivation layer. The local acidification is so efficient that the primary passive film is dissolved and active sulfide-mediated dissolution of the metal occurs, as has been proposed for acidic solutions containing H_2S [14,21,73,74]:

$$M + HS^- \rightarrow MHS_{ads} + e^- \tag{7}$$

$$MHS_{ads} \rightarrow MHS_{ads}^+ + e^- \tag{8}$$

$$MHS_{ads}^+ \rightarrow M_{aq}^{2+} + HS^- \tag{9}$$

4. Conclusions

In the present work, the effect of temperature and concentration of sulfide ions on the corrosion behavior of AISI 304L and AISI 316L stainless steels in seawater was studied. The results can be summarized as follows.

The corrosion resistance of 304L and 316L stainless steels at E_{OC} is due to the formation of a natural surface film. It was found that the stability (resistance, compactness, and thickness) of the surface film decreases with increasing temperature and sulfide ions. In addition, sulfurization of the surface film most likely occurs in the presence of sulfide ions.

An increase in seawater temperature and pollutant concentration has a negative effect on the corrosion stability of stainless steel; therefore, the corrosion potential shifts toward the cathodic side, and the corrosion current increases. In the passive potential region,

the passivation current increases, the depassivation potential decreases, and the passive potential region narrows.

The occurrence of pitting corrosion on the surface of stainless steel was confirmed with non-contact 3D profilometer analysis. Fewer large pits (depth 80–100 μm and width 100 μm) are formed on the surface of AISI 304L steel, while a larger number of smaller pits (depth 40–50 μm and width 50 μm) are formed on the surface of AISI 316L steel. With increasing temperature and sulfide ion concentration, the width, depth, and density of the pits increase in both steel samples.

In the observed temperature range (from 288 to 308 K) and sulfide ion concentration (up to 40 ppm), the AISI 316L steels exhibit higher corrosion resistance. The influence of sulfide ions on steel corrosion is more pronounced than the influence of temperature.

Author Contributions: Conceptualization, S.G. and L.V.; methodology, S.G. and L.V.; software, S.G., J.K. and A.N.; validation, S.G. and E.E.O.; formal analysis, S.G., J.K. and A.N.; investigation, A.M., L.V., S.G. and A.N.; resources, A.M., L.V., S.G. and J.K.; data curation, L.V., J.K. and A.N.; writing—original draft preparation, S.G., L.V., A.M., E.E.O. and J.K.; writing—review and editing, S.G., L.V., E.E.O. and A.N.; visualization, S.G., J.K. and A.N.; supervision, S.G.; project administration, S.G.; funding acquisition, S.G. and L.V. All authors have read and agreed to the published version of the manuscript.

Institutional Review Board Statement: Not applicable.

Informed Consent Statement: Not applicable.

Data Availability Statement: The data presented in this study are available on request from the corresponding author.

Conflicts of Interest: The authors declare no conflict of interest.

References

1. Al-Fozan, S.A.; Malik, A.U. Effect of seawater level on corrosion behavior of different alloys. *Desalination* **2008**, *228*, 61–67. [CrossRef]
2. Chen, J.; Zhang, Q.; Li, Q.; Fu, S.-L.; Wang, J.-Z. Corrosion and tribocorrosion behaviors of AISI 316 stainless steel and Ti6Al4V in artificial seawater. *Trans. Nonferrous Met. Soc. China* **2014**, *24*, 1022–1031. [CrossRef]
3. Carvalho, M.L. Corrosion of Copper Alloys in Natural Seawater: Effects of Hydrodynamics and pH. Ph.D. Thesis, Université Pierre et Marie Curie, Paris, France. Available online: https://theses.hal.science/tel-01207012 (accessed on 25 March 2023).
4. Kovač, N.; Ivošević, Š.; Vastag, G.; Vukelić, G.; Rudolf, R. Statistical approach to the analysis of the corrosive behaviour of NiTi alloys under the influence of different seawater environments. *Appl. Sci.* **2021**, *11*, 8825. [CrossRef]
5. Ivošević, Š.; Kovač, N.; Momčilović, N.; Vukelić, G. Evaluation of the corrosion depts of a double bottom longitudinal girder on aging bulk carriers. *J. Mar. Sci. Eng.* **2022**, *10*, 1425. [CrossRef]
6. Wiener, M.; Salas, B.V. Corrosion of the marine infrastructure in polluted seaports. *Corros. Eng. Sci. Technol.* **2005**, *40*, 137–142. [CrossRef]
7. Valdez, B.; Ramirez, J.; Eliezer, A.; Schorr, M.; Ramos, R.; Salinas, R. Corrosion assessment of infrastructure assets in coastal seas. *J. Mar. Eng. Technol.* **2016**, *15*, 124–134. [CrossRef]
8. Zhu, J.; Li, D.; Chang, W.; Wang, Z.; Hu, L.; Zhang, Y.; Wang, M.; Yang, Z.; Song, J.; Chen, S.; et al. In situ marine exposure study on corrosion behaviors of five alloys in coastal waters of western Pacific Ocean. *J. Mater. Res. Technol.* **2020**, *9*, 8104–8116. [CrossRef]
9. Valdez, B.; Schorr, M.; Quintero, M.; Garcia, R.; Rosas, N. Effect of climate change on durability of engineering materials in hydraulic infrastructure: An overview. *Corros. Eng. Sci. Technol.* **2010**, *45*, 34–41. [CrossRef]
10. Roberge, P.R. Impact of climate change on corrosion risks. *Corros. Eng. Sci. Technol.* **2010**, *45*, 27–33. [CrossRef]
11. Wiener, M.S.; Salas, B.V.; Quintero-Nunez, M.; Zlatev, R. Effect of H_2S on corrosion in polluted waters: A review. *Corros. Eng. Sci. Technol.* **2006**, *41*, 221–227. [CrossRef]
12. Fernandez-Domene, R.M.; Sanchez-Tovar, R.; Escriva-Cerdan, C.; Leiva-Garcia, R.; Garcia-Anton, J. Comparison of the effect of non-polluted and underwater volcano polluted seawater on the corrosion resistance of different stainless steels. *Mater. Corros.* **2015**, *66*, 1279–1288. [CrossRef]
13. Siang, H.Y.; Tahir, N.M.; Malek, A.; Isa, M.A.M. Breakdown of hydrogen sulfide in seawater under different ratios of dissolved oxygen/hydrogen sulfide. *Malaysian J. Anal. Sci.* **2017**, *21*, 1016–1027. [CrossRef]

14. Betova, I.; Bojinov, M.; Hyökyvirta; Saario, T. Effect of sulphide on the corrosion behavior of AISI 316L stainless steel and its constituent elements in simulated Kraft digester conditions. *Corros. Sci.* **2010**, *52*, 1499–1507. [CrossRef]

15. Yuan, S.; Liang, B.; Pehkonen, S.O. Surface chemistry and corrosion behaviour of 304 stainless steel in simulated seawater containing inorganic sulphide and sulphate reducing bacteria. *Corros. Sci.* **2013**, *74*, 353–366. [CrossRef]

16. Boyapati, V.A.R.; Kanukula, C.K. Corrosion inhibition of Cu-Ni (90/10) alloy in seawater and sulphide polluted seawater environments by 1,2,3-benzotriazole. *Int. Sch. Res. Not.* **2013**, *2013*, 703929. [CrossRef]

17. Syrett, B.C. The mechanisms of accelerated corrosion of copper-nickel alloys in sulfide-poluted seawater. *Corros. Sci.* **1981**, *21*, 187–209. [CrossRef]

18. Traverso, P.; Beccaria, A.M.; Poggi, G. Effect of sulphides on corrosion of Cu-Ni-Fe-Mn alloy in sea water. *Br. Corros. J.* **1994**, *29*, 110–114. [CrossRef]

19. Szyprowski, A.J. Sulphide corrosion of alloy steels in chloride solutions: Potentiokinetic investigations. *Br. Corros. J.* **1998**, *33*, 103–110. [CrossRef]

20. Dexter, S.C. *Sea-Water Corrosion*; ASM International: Materials Park, OH, USA, 1987; Volume 13, pp. 346–893.

21. Ma, H.; Cheng, X.; Li, G.; Chen, S.; Quan, Z.; Zhao, S.; Niu, L. The influence of hydrogen sulphide on corrosion of iron under different conditions. *Corros. Sci.* **2000**, *42*, 1669–1683. [CrossRef]

22. Zhao, W.; Zou, Y.; Matsuda, K.; Zou, Z. Characterization of the effect of hydrogen sulfide on the corrosion of X80 pipeline steel in saline solution. *Corros. Sci.* **2016**, *102*, 455–468. [CrossRef]

23. Baddoo, N.R. Stainless steel in construction: A review of research, applications, challenges and opportunities. *J. Constr. Steel. Res.* **2008**, *64*, 1199–1206. [CrossRef]

24. Jessen, C.Q.; Jensen, E.O. *Stainless Steel for Hygienic Equipment in Food/Pharma*; Damstahl: Skanderborg, Denmark, 2015.

25. Kožuh, S.; Gojić, M.; Vrsalović, L.; Ivković, B. Corrosion failure and microstructure analysis of the AISI 316L stainless steels for ship pipeline before and after welding. *Kovove. Mater.* **2013**, *51*, 53–61. [CrossRef]

26. Gudić, S.; Nagode, A.; Šimić, K.; Vrsalović, L.; Jozić, S. Corrosion behavior of different types of stainless steel in PBS solution. *Sustainability* **2022**, *14*, 8935. [CrossRef]

27. Naha, S.K. Stainless Steel the Green Alloy. *Sci. Rep.* **2011**, *48*, 52–55. Available online: https://nopr.niscpr.res.in/bitstream/1234 56789/11420/1/SR%2048%284%29%2052-55.pdf (accessed on 25 March 2023).

28. Juraga, I.; Šimunović, V.; Španiček, Đ. Contribution to the study of effects of surface state of welded joints in stainless steel upon resistance towards pitting corrosion. *METABK* **2007**, *46*, 185–189.

29. Mandrino, D.J.; Godec, M.; Torkar, M.; Jenko, M. Study of oxide protective layers on stainless steel by AES, EDS and XPS. *Surf. Interface Anal.* **2008**, *40*, 285–289. [CrossRef]

30. Olsson, C.O.A.; Landolt, D. Passive films on stainless steels—chemistry, structure and growth. *Electrochem. Acta* **2003**, *48*, 1093–1104. [CrossRef]

31. Matsch, S.; Suter, T.; Bohni, H. Microelectrochemical investigations of stainless steels at elevated temperatures. *Mater. Sci. Forum.* **1998**, *289–292*, 1127–1138. [CrossRef]

32. Matsch, S.; Bohni, H. Influence of temperature on the localized corrosion of stainless steels. *Russ. J. Electrochem.* **2000**, *36*, 1268–1274. [CrossRef]

33. Kashkowski, R.; Strelnikova, K.; Fedotova, A. Application of electrochemical impedance spectroscopy to study hidrgen sulphide corrosion of steel and its inhibition: A review. *Corros. Eng. Sci. Technol.* **2019**, *54*, 493–515. [CrossRef]

34. Wang, Z.; Zhang, L.; Zhang, Z.; Lu, M. Combined effect of pH and H_2S on the structure of passive film formed on type 316L stainless steel. *Appl. Surf. Sci.* **2018**, *458*, 686–699. [CrossRef]

35. Mat, S.; Newman, R. *Local Chemistry Aspects of Hydrogen Sulphide Assisted SCC of Stainless Steel*; Corrosion 1994 Paper no. 228; NACE Int.: Houston, HI, USA, 1994.

36. Marcus, P. Sulfur-assisted corrosion mechanisms and the role of alloyed elements. In *Corrosion Mechanisms in Theory and Practice*; Marcus, P., Ed.; Marcel Dekker, Inc.: New York, NY, USA, 2002.

37. Ding, J.; Zhang, M.; Wang, J.; Wen, Z.; Hao, W. The electrochemical behavior of 316L austenitic stainless steel in Cl⁻ containing environment under different H_2S partial pressures. *Appl. Surf. Sci.* **2014**, *289*, 33–41. [CrossRef]

38. Sobral, A.V.C.; Ristov, W., Jr.; Azambuja, D.S.; Costa, I.; Franco, C.V. Potentiodynamic tests and electrochemical impedance spectroscopy of injection molded 316L steel in NaCl solution. *Corros. Sci.* **2001**, *43*, 1019–1030. [CrossRef]

39. Yu, X.; Al-Saadi, S.; Zhao, X.-L.; Raman, R.K.S. Electrochemical investigations of steels in seawater sea sand concrete environments. *Materials* **2021**, *14*, 5713. [CrossRef] [PubMed]

40. Yuan, S.J.; Pehkonen, S.O.; Ting, Y.P.; Kang, E.T.; Neoh, K.G. Corrosion behavior of type 304 stainless steel in a simulated seawater-based medium in the presence and absence of aerobic Pseudomonas NCIMB 2021 bacteria. *Ind. Eng. Chem. Res.* **2008**, *47*, 3008–3020. [CrossRef]

41. Wan, D.; Yuan, S.J.; Neoh, K.G.; Kang, E.T. Poly(glycidyl methacrylate)–polyaniline bilayer-modified mild steel for combating biocorrosion in seawater. *J. Electrochem. Soc.* **2009**, *156*, C266–C274. [CrossRef]

42. Donik, Č.; Kocijan, A. Comparison of the corrosion behaviour of austenitic stainless steel in seawater and in a 3.5 % NaCl solution. *Mater. Technol.* **2014**, *48*, 937–942.

43. Nie, J.; Wei, L.; Jiang, Y.; Li, Q.; Luo, H. Corrosion mechanism of additively manufactured 316L stainless steel in 3.5 wt.% NaCl solution. *Mater. Today Commun.* **2021**, *26*, 101648. [CrossRef]

44. Raistrick, I.D.; Macdonald, J.R.; Franceschetti, D.R. *Impedance Spectroscopy*; Macdonald, J.R., Ed.; Wiley & Sons: New York, NY, USA, 1987.

45. Rammelt, U.; Reinhard, G. On the applicability of a constant phase element (CPE) to the estimation of roughness of solid metal electrodes. *Electrochim. Acta* **1990**, *35*, 1045–1049. [CrossRef]

46. Zatkalikova, V.; Markovičova, L. Influence of temperature on corrosion resistance of austenitic stainless stell in Cl- containing solutions. *Prod. Eng. Arch.* **2019**, *25*, 43–46. [CrossRef]

47. Chen, J.; Zhou, Q.; Liu, Y.; Ma, Y.; Yin, J.; Hu, T.; Li, Y. Influence of temperature on the corrosion behavior of 18Mn-18Cr austenitic stainless steel in 3.5 wt.% NaCl solution. *Int. J. Electrochem. Sci.* **2022**, *17*, 22105. [CrossRef]

48. Zhiyuan, Z. Effect of sulphide addition to chloride environment on corrosion behavior of SAF2507 duplex stainless steel. *Int. J. Electrochem. Sci.* **2016**, *11*, 10895–10905. [CrossRef]

49. Hesketh, J.; Dickinson, E.J.F.; Martin, M.L.; Hinds, G.; Turnbull, A. Influence of H_2S on the pitting corrosion of 316L stainless steel in oilfield brine. *Corros. Sci.* **2021**, *182*, 109265. [CrossRef]

50. Ge, H.-H.; Zhoua, G.-D.; Wub, W.-Q. Passivation model of 316 stainless steel in simulated cooling water and the effect of sulfide on the passive film. *Appl. Surf. Sci.* **2003**, *211*, 321–334. [CrossRef]

51. He, W.; Knudsen, O.Ø.; Diplas, S. Corrosion of stainless steel 316L in simulated formation water environment with CO_2–H_2S–Cl^-. *Corros. Sci.* **2009**, *51*, 2811–2819. [CrossRef]

52. Moreno, D.A.; De Mele, M.F.L.; Ibars, J.R.; Videla, H.A. Influence of microstructure on the electrochemical behavior of type 410 stainless steel in chloride media with inorganic and biogenic sulfide. *Corrosion* **1991**, *47*, 2–9. [CrossRef]

53. Adebayo, A.; Oluwadare, B.S. Corrosion of steels in water and hydrogen sulphide. *Rev. of Ind. Eng. Lett.* **2014**, *1*, 80–88. [CrossRef]

54. Chen, S.; Cheng, Y.F.; Voordouw, G.A. Comparative study of corrosion of 316L stainless steel in biotic and abiotic sulfide environments. *Int. Biodeterior. Biodegrad.* **2017**, *120*, 91–96. [CrossRef]

55. Gramp, J.P.; Bigham, J.M.; Jones, F.S.; Tuovinen, O.H. Formation of Fe-sulfides in cultures of sulfate-reducing bacteria. *J. Hazard. Mater.* **2010**, *175*, 1062–1067. [CrossRef]

56. Duan, J.; Hou, B.; Yu, Z. Characteristics of sulfide corrosion products on 316L stainless steel surfaces in the presence of sulfate-reducing bacteria. *Mater. Sci. Eng. C Bio. S.* **2006**, *26*, 624–629. [CrossRef]

57. Remazeilles, C.; Saheb, M.; Neff, D.; Guilminot, E.; Tran, K.; Bourdoiseau, J.A.; Sabot, R.; Jeannin, M.; Matthiesen, H.; Dillmann, P.; et al. Microbiologically influenced corrosion of archaeological artifacts: Characterization of iron(II) sulfides by Raman spectroscopy. *J. Raman Spectrosc.* **2010**, *41*, 1425–1433. [CrossRef]

58. Stern, M.; Geary, A.L. Electrochemical polarization: I. A theoretical analysis of the shape of polarization curves. *J. Electrochem. Soc.* **1957**, *104*, 56–63. [CrossRef]

59. Williams, D.E.; Wright, G.A. Nucleation and growth of anodic oxide films on bismuth—I. Cyclic voltammetry. *Electrochim. Acta* **1976**, *21*, 1009–1019. [CrossRef]

60. Malik, A.U.; Mayan Kutty, P.C.; Siddiqi, N.A.; Andijani, I.N.; Ahmed, S. The influence of pH and chloride concentration on the corrosion behaviour of AISI 316L steel in aqueous solutions. *Corros. Sci.* **1992**, *33*, 1809–1827. [CrossRef]

61. Park, J.O.; Matsch, S.; Bohni, H. Effects of temperature and chloride concentration on pit initiation and early pit growth of stainless steel. *J. Electrochem. Soc.* **2002**, *149*, B34–B39. [CrossRef]

62. Marcus, P. Surface science approach of corrosion phenomena. *Electrochim. Acta* **1998**, *43*, 109–118. [CrossRef]

63. Wilde, B.E. Critical appraisal of some popular laboratory electrochemical tests for predicting the localized corrosion resistance of stainless alloys in sea water. *Corrosion* **1972**, *28*, 283–291. [CrossRef]

64. Silverman, D.C. Electrochemical techniques—simple tests for complex predictions in the chemical process industries. *Corros. Rev.* **1992**, *10*, 31–78. [CrossRef]

65. Babolan, R. *Corrosion Tests and Standards, Application and Interpretation*, 2nd ed.; ASTM International: West Conshohochen, PA, USA, 2005.

66. Pardo, A.; Merino, M.C.; Coy, A.E.; Viejo, F.; Arrabal, R.; Matykina, E. Pitting corrosion behavior of austenitic stainless steels—combining effects of Mn and Mo additions. *Corros. Sci.* **2008**, *50*, 1796–1806. [CrossRef]

67. Valero Vidal, C.; Igual Munoz, A. Electrochemical characterization of biomedical alloy for surgical implants in simulated body fluids. *Corros. Sci.* **2008**, *50*, 1954–1961. [CrossRef]

68. Ha, H.-Y.; Lee, T.-H.; Bae, J.-H.; Chun, D.W. Molybdenum effects on pitting corrosion resistance of FeCrMnMoNC austenitic stainless steel. *Metals* **2018**, *8*, 653. [CrossRef]

69. Wang, Z.; Paschalidou, E.-M.; Seyeux, A.; Zanna, S.; Maurice, V.; Marcus, P. Mechanisms of Cr and Mo enrichments in the passive oxide film on 316L austenitic stainless steel. *Front. Mater.* **2019**, *6*, 232. [CrossRef]

70. Wang, Z.; Di-Franco, F.; Seyeux, A.; Zanna, S.; Maurice, V.; Marcus, P. Passivation-induced physicochemical alterations of the native surface oxide film on 316L austenitic stainless steel. *J. Electrochem. Soc.* **2019**, *166*, C3376–C3388. [CrossRef]

71. Leising, C. Pitting corrosion measurement using 3D profilometry. *Tech. Rep.* **2014**. [CrossRef]

72. Hansson, E.B.; Odziemkowski, M.S.; Gillham, R.W. Formation of poorly crystalline iron monosulfides: Surface redox reactions on high purity iron, spectroelectrochemical studies. *Corros. Sci.* **2006**, *48*, 3767–3783. [CrossRef]

73. Shoesmith, D.W.; Taylor, P.; Bailey, M.G.; Ikeda, B. Electrochemical behaviour of iron in alkaline sulphide solutions. *Electrochim. Acta* **1978**, *23*, 903–916. [CrossRef]

74. Ma, H.; Cheng, X.; Chen, S.; Wang, C.; Zhang, J.; Yang, H. An ac impedance study of the anodic dissolution of iron in sulfuric acid solutions containing hydrogen sulfide. *J. Electroanal. Chem.* **1998**, *451*, 11–17. [CrossRef]